Experimental evidence of the effect of heat flux on Thomson scattering off ion acoustic waves

F. Amiranoff,[1] S. D. Baton,[1] S. Hüller,[2] V. Malka,[1] A. Modena,[1] Ph. Mounaix,[2] N. Renard-Le Galloudec,[3,*] C. Rousseaux,[3,†] and M. Salvati[1]

[1]*LULI, UMR No. 7605, CNRS, CEA, Ecole Polytechnique, Université Pierre et Marie Curie, 91128 Palaiseau Cedex, France*

[2]*CPhT, CNRS, Ecole Polytechnique, 91128 Palaiseau Cedex, France*

[3]*CEA Limeil-Valenton, 94195 Villeneuve-St.-Georges Cedex, France*

(Received 30 August 1999)

Thomson self-scattering measurements are performed in a preionized helium gas jet plasma at different locations along the laser propagation direction. A systematic and important variation of the intensity ratio between the blue and the red ion spectral components is observed, depending on whether the location of the probed region is in front of or behind the focal plane. A simple theoretical calculation of Thomson scattering shows that this behavior can be qualitatively understood in terms of a deformation of the electron distribution function due to the return current correlated with the classical thermal heat flux.

PACS number(s): 52.40.Nk, 52.35.Fp, 52.50.Jm

I. INTRODUCTION

When heated by a high-intensity laser beam, a plasma generally presents large temperature gradients. These gradients give rise to a correspondingly large heat flux associated with a deformation of the electron distribution function from its equilibrium Maxwellian shape [1]. The precise description of the electron heat transport in laser-produced plasma is of importance for many applications relying on laser-plasma interaction physics, such as inertial confinement fusion or x-ray lasers. In a homogeneous plasma and for modest temperature gradients (when the thermal electron collisional mean-free-path is much smaller than the temperature gradient length: $\lambda_t \ll L_T$), the heat flux is calculated by a first order perturbation of the distribution function and it is proportional to the local temperature gradient [1]. When $\lambda_t / L_T > 0.002$, the mean free path of the electrons participating most in the heat flux becomes comparable to the gradient length and this local approach is no longer valid. A nonlocal description has been developed in which the local heat flux at a given position in the plasma depends on the whole temperature profile in the surrounding region [2]. An experimental access to the distribution function is through Thomson scattering on thermal fluctuations.

Thomson scattering is a powerful diagnostic technique for measuring the parameters of a plasma [3–6]. By irradiating the plasma with a laser probe beam and by measuring the spectrum of the light scattered by the electrons one has access to some part of the density fluctuation spectrum. From this, it is possible to measure the electron temperature and density T_e and n_e, the ion temperature T_i, the plasma flow velocity as well as the drift velocity between electrons and ions. Some examples are found in Refs. [7–15]. The effect of heat flux is more readily observed when measuring the spectrum of the fluctuations near the ion-acoustic frequency ω_{iaw}. In an equilibrium plasma and in a geometry where collective scattering is observed, it consists of two equal amplitude satellites at $\omega_{\rm pr} \pm \omega_{iaw}$ where $\omega_{\rm pr}$ is the frequency of the probe beam [6]. These satellites at frequencies $\omega_{\rm pr} \pm \omega_{\rm iaw}$ correspond, respectively, to fluctuations with wave numbers $\mathbf{k}_{\rm iaw} = \pm(\mathbf{k}_{\rm scat} - \mathbf{k}_{\rm pr})$, where $\mathbf{k}_{\rm scat}$ and $\mathbf{k}_{\rm pr}$ are the wave numbers of the scattered beam and the probe beam, respectively. Because of the deformation of the electron distribution function due to heat flux (often accounted for as a relative drift velocity between electrons and ions), the plasma susceptibility is different for these two ion-acoustic fluctuations and the two satellites have different intensities [6]. This effect is commonly explained as a difference in the electron Landau damping term in the shifted electron distribution for the two ion-acoustic wave numbers. This asymmetry between the blue and red satellites has already been observed in several experiments and qualitatively explained in terms of drift velocity and electron heat flux [7,10,14].

In this paper we present a comprehensive study of this blue/red asymmetry in the ion acoustic scattered spectrum in a well diagnosed quasihomogeneous stationary plasma. As expected in a plasma with symmetric temperature and density profiles, we observe a symmetric variation of the ratio between the two satellites on each side of the hottest region. These results are well reproduced by calculating the first order correction to the electron distribution function for a 1D temperature gradient (along the laser propagation axis) and the corresponding plasma susceptibility for the measured plasma parameters. Nevertheless, this good quantitative agreement is only obtained with an ion temperature significantly lower than estimated from hydrodynamic simulations.

II. EXPERIMENTAL SETUP

The experiment was performed using two beams of the multibeam laser facility at the Laboratoire pour l'Utilisation des Lasers Intenses (LULI). The laser pulses are Gaussian in time with a duration of 600 ps full width at half maximum (FWHM). Figure 1 shows the experimental configuration. The creation beam used to preionize the plasma was operated at the fundamental frequency of the Nd:glass laser (1.053

*Present address: Department of Physics/220, University of Nevada-Reno, Reno, NV 89557-0058.

†Present address: CEA Bruyères-le-Châtel, DCRE/CSE, BP 12, 91680 Bruyères-le-Châtel, France.

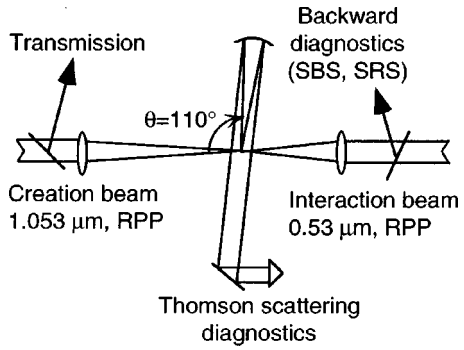

FIG. 1. Experimental setup.

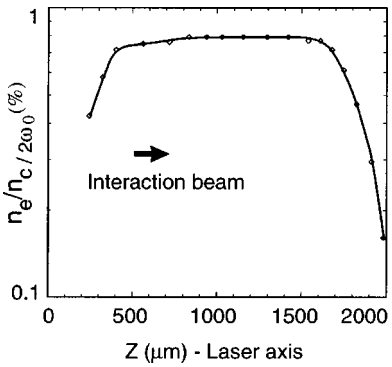

FIG. 2. Experimental electron density profile. The origin in z is arbitrary. The interaction beam comes from the left.

μm). It was focused with a $f/6$ aperture lens at the center of a cylindrical supersonic helium gas jet of 2.5 mm in diameter. This beam was spatially smoothed by a 8 mm cell Random Phase Plate (RPP) giving a spatially averaged intensity of $4\times10^{14}\,\mathrm{W/cm^2}$. The gas was fully ionized by collisional ionization along the whole length of the jet perpendicular to the gas flow.

The interaction beam, at twice the fundamental frequency (0.526 μm), was fired in the opposite direction to the creation beam after a time delay of 1 ns (this delay corresponds to the time between the maxima of the pulses). This beam was focused with a $f/3$ aperture lens (250-mm focal length) at the center of the jet and was spatially smoothed by either a 0.65 mm cell RPP or a 2.1-mm cell RPP. The maximum energy of the interaction beam was 30 J. In the following, the mean experimental intensity is defined as the ratio of 80% of the incident energy over 600-ps duration and averaged in the Airy focal spot (diameter between the first Airy minima). This gave a maximum intensity of $2\times10^{13}\,\mathrm{W/cm^2}$ for the 0.65-mm cell RPP and $2\times10^{14}\,\mathrm{W/cm^2}$ for the 2.1-mm cell RPP. The focal spot images, obtained in transmission in vacuum, were in agreement with the calculated ones (diameter of 500 μm for the 0.65-mm cell RPP, and 150 μm for the 2.1-mm cell RPP).

The self-scattering Thomson spectra (the probe beam is the 0.526 μm interaction beam itself) were obtained at a scattering angle $\theta=110°$ from the interaction laser beam axis. The scattered light was collected by reflective optics. It was imaged with a $f/3$ spherical mirror and a 1:5 magnification onto the entrance slit of a 1 m spectrometer for the ion acoustic waves (IAW) and a 0.35 m spectrometer for the electron plasma waves (EPW). The spectra were recorded with optical streak cameras coupled with CCD cameras: the IAW spectra were obtained with a very high spectral resolution (0.5 Å) and the EPW spectra, with a low spectral dispersion in order to record the up and down components. The electron density inside ±500 μm from the center of the jet was deduced from the scattered signal on the EPW at different locations along the interaction axis. Beyond this region, the intensity of the scattered signal was too weak and we inferred the electron density from a previous study [16] in which a beam at $2\omega_0$ interacted with the Helium gas jet. In this study, the EPW self-scattering Thomson spectrum was spatially resolved by using an optical device that rotates the image of the plasma by 90° along the slit of the low dispersion imaging spectrometer, and by setting a low sweep speed on the streak camera and removing its entrance slit. Due to the absence of time resolution, the collected signal was strong enough to obtain, on one laser shot, the spatial profile of the electron density along the laser axis up to ±1 mm from the center of the jet. We have checked that the two electron density profiles coincide over the central region (i.e., inside ±500 μm from the center of the jet), which confirms that in our experimental conditions the electron density does not depend sensitively on the plasma creation conditions.

III. EXPERIMENTAL RESULTS

For reader convenience we show in Fig. 2 a typical electron density profile obtained from [16]. The origin in z is arbitrary. One can see a very flat electron density profile over 1.5 mm. Typically, with a backing pressure of 65 bars, the plasma is quasihomogeneous with an electron density around $3.5\times10^{19}\,\mathrm{cm^{-3}}$. The asymmetry of the region within which the electron density profile is well described comes from the attenuation of the beam due to its propagation through the gas. This damping results in a weaker scattered signal on the outgoing side of the beam compared to the incoming side.

Other diagnostics were set up for this experiment. In particular, measurements and analysis of the backscattered light of the interaction beam (collected through the focusing lens) have allowed us to obtain the values of the stimulated Brillouin (SBS) and Raman (SRS) scattering reflectivities in the backward direction. The SBS reflectivities were between 5×10^{-3} and 10^{-2} for the 2.1-mm cell RPP (at intensity of $2\times10^{14}\,\mathrm{W/cm^2}$) and remained below 10^{-5} for the 0.65-mm cell RPP (at intensity of $2\times10^{13}\,\mathrm{W/cm^2}$), the SRS ones never exceeded 10^{-5}. The transmission rate ranged between 70% and 80 %.

The most striking result is presented in Fig. 3 which shows Thomson self-scattering time-resolved spectra on IAW recorded at different positions along the interaction axis for the 0.65 mm cell RPP: -1500 μm, -1000 μm, -500 μm, center, $+500$ μm and $+1000$ μm from the jet center. Similar spectra, not shown here, have been obtained with the 2.1 mm cell RPP. Each image has been obtained in the same experimental conditions with the same combination of filters and optical attenuators. The central spectral feature corresponds to the laser noise at $2\omega_0$ (0.526 μm). The two other spectral components on both sides correspond to Thomson self-scattering on the IAW. During the interaction time, these two satellites move apart slightly, which shows that the interaction beam weakly heats the plasma. The most

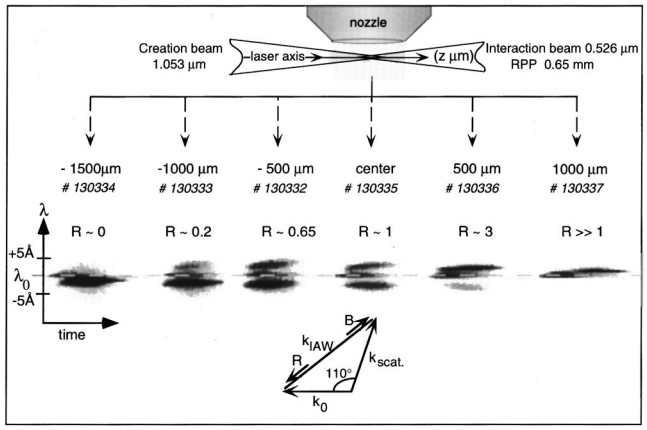

FIG. 3. Thomson scattering time-resolved spectra on IAW for the 0.65 mm RPP. Each spectrum is obtained at different positions along the laser axis and with the same conditions. The diagnostic geometry is represented on the top of the figure and the geometry of the different wave numbers involved at the bottom. On each spectrum, one can see the ratio $R(R=I_B/I_R)$ between the intensity of the blue component (I_B) and the red one (I_R).

remarkable result is the ratio between the two components. When moving away from the center of the gas jet, one of the two satellites becomes predominant: on the incoming side of the interaction beam the red satellite dominates while on the outgoing side the blue one dominates. On each spectrum, we have indicated the intensity ratio R between the red component (I_R) and the blue one (I_B), where $R=I_R/I_B$. At the bottom of Fig. 3 one can see the scheme of the three different wave numbers where $\mathbf{k}_0$ denotes the incident laser wave number, $\mathbf{k}_{\rm scat}$ the scattering wave number and $\mathbf{k}_{\rm IAW}$ the IAW wave number with the red and the blue components. This result is very reproducible for both RPP's. The only significant difference we have observed is that, in the case of the 2.1 mm RPP, the red satellite is dominant at the center of the jet, unlike what is observed with the 0.65-mm RPP where the two satellites are comparable. This effect might be attributed to a non-negligible side-SBS induced amplification of the red component for the 2.1 mm RPP. Such an interpretation is supported by the difference observed in the backward SBS reflectivities with the two RPP's. From these spectra, we have estimated the electron temperature profile along the interaction axis. Figure 4 shows the electron temperature profile thus obtained from Fig. 3. This temperature has been determined at the incoming time of the interaction pulse. The horizontal error bars correspond to the uncertainty on the localization of the center of the interaction region. The vertical ones correspond to the somewhat arbitrariness of the definition of the incoming time of the interaction pulse and to the width of the spectra.

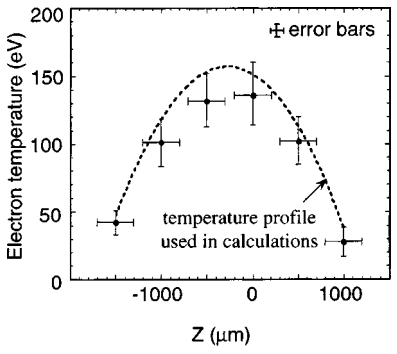

FIG. 4. Experimental electron temperature profile in the interaction condition of the 0.65 mm RPP (●). The dashed line corresponds to the temperature profile taken in the theoretical calculation.

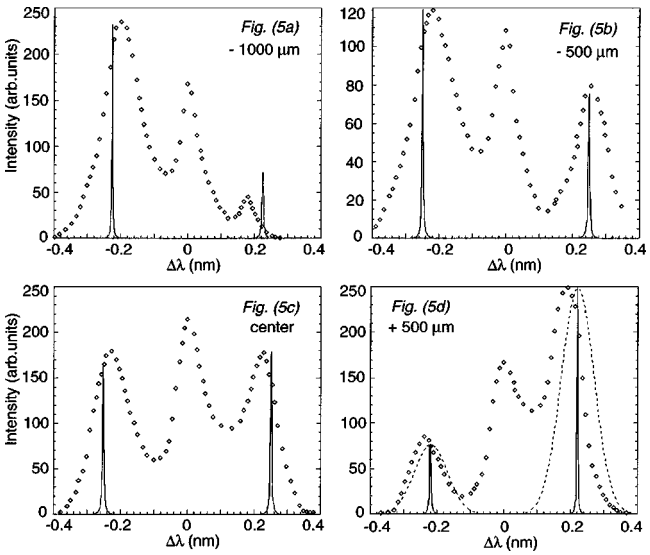

FIG. 5. Experimental (◇) and theoretical (plain line) spectra for the 0.65 mm cell RPP at four locations: -1000 μm (a), -500 μm (b), center (c), and $+500$ μm (d) in arbitrary units. The electron temperature corresponds to the dashed line in Fig. 4 and the ion temperature is assumed to be equal at 10 eV. The dashed line represented in (d) corresponds to the theoretical spectra calculated with a typical instrumental resolution of 0.5 Å.

IV. DISCUSSION

A number of calculations have been made which take into account the electron heat flux and its effect on the ion acoustic waves and their Thomson scattering spectra (e.g., [17,18]). In our case the typical ratio between the electron mean free path and the temperature gradient scale length is of the order of $\lambda_t/L_T \approx 3$ μm/1000 μm$=3\times10^{-3}$ so that the local theory is at the edge of its domain of validity. Thus, in order to explain the experimental spectra we have performed a simple theoretical calculation of Thomson scattering which takes into account the electron and ion temperature profiles in the longitudinal direction. The radial variation of the electron temperature has been neglected assuming that the thermal transport is effective enough for the electron temperature to be nearly constant throughout the focal spot (transversally) at the arrival time of the interaction beam. The electron and ion velocity distribution functions to be implemented in the Thomson scattering dynamical form factor have been computed at the first order of the classical Chapman-Enskog [19] scheme. The collision operator has been taken to be the simplest Bhatnagar-Gross-Krook (BGK) [20] operator. Although not presented here, we have also obtained very close results with the Lorentz collisional operator in the low frequency limit which is valid here.

Figure 5 shows the experimental and theoretical spectra in arbitrary units for the 0.65 mm cell RPP at four locations

between -1000 μm and $+500$ μm. To compare the theoretical and experimental peak ratios (which is the important quantity) easily, we have adjusted the theoretical and experimental units so that the height of the most intense peaks coincide. Let us mention that the width of the experimental spectra is due to the instrumental resolution which has not been taken into account in the theoretical calculations since it does not modify the peak intensity ratio. As an example, we show on Fig. 5(d) (dashed line) a theoretical spectrum with a typical instrumental resolution of 0.5 Å. As previously explained, we have also adjusted the height of the peaks. The electron density corresponds to the experimental value ($n_e = 3.5\times 10^{19}\,\mathrm{cm}^{-3}$). The electron temperature we have taken for the theoretical spectra corresponds to the dashed line in Fig. 4, i.e., T_e varying from 160 to 50 eV over 1200 μm with a typical gradient length of $L_T = 1000\,\mu$m when $T_e = 120$ eV. A large asymmetry between the red and blue components is only possible when the ion Landau damping is negligible with respect to the electron Landau damping. This is obtained in helium ($Z=2$) for $ZT_e/T_i \geqslant 17$ [21]. Thus we assumed an ion temperature of $T_i = 10$ eV. We verified that, as expected, the experimental results could not be reproduced for larger ion temperatures.

We have adjusted the parameters within a reasonable range in order to obtain peak intensity ratios comparable to the experimental ones. In order for the theoretical and experimental spectra to be in reasonable agreement, we had to fit the electron temperature profile to the upper limit within the error bars. The computation of the spectra based on our theoretical model shows (see Fig. 5) a satisfying agreement with the experimental spectra in particular for the peak intensity ratios. The agreement of the case shown in Fig. 5(a) where the experimental ratio R is overestimated by a factor of 1.6 is less convincing; this discrepancy can be attributed to an increasing error in the determination of the plasma parameters when approaching the edge of the gas jet. For this reason data recorded at -1500 μm and $+1000$ μm are of minor reliability and the comparison between theory and experiment is not shown here. It can be seen that while the peak intensity ratio is well reproduced, the experimental peak separation (i.e., the electron temperature) is slightly less than the theoretical one. This suggests that the simplest classical model of heat transport does not allow us to find a single set of parameters yielding at the same time both a satisfactory theoretical peak ratio and the peak separation. The small global spectral shift towards longer (shorter) wavelengths that can be observed on the -500 μm ($+500$ μm) spectrum might be explained in terms of Doppler shift due to a small radial (outward) component of the jet velocity.

As already mentioned, the calculated spectra reproduce the essential features of the experimental spectra (i.e., predominance of the red or blue line depending on the location of the scattering region with a ratio R in the same order than the experimental one) provided the ion temperature T_i is less than around 10 eV. Such an ion temperature is less than the one deduced from the hydrocode MULTI [22] which gave $T_i = 30-40$ eV for which our theoretical calculations yield no significant effect on the Thomson scattering spectrum. It follows that these preliminary theoretical estimates might quantitatively explain our results if some process relevant for the ion thermal transport in our experimental conditions could be found to be missing in the hydrocode simulations, so that the actual ion temperature would indeed be less than the calculated value. Another interesting possibility to investigate would be that the ''microscopic'' speckle structure of the smoothed interaction beam modifies the electron distribution function drastically, which would invalidate our use of a naive classical Chapman-Enskog scheme (e.g. [17]). For the sake of completeness, let us also mention that in our experimental conditions, we may expect a non-Maxwellian zero-order electron distribution function at intensities higher than around $10^{15}\,\mathrm{W/cm}^2$ [23]. This effect will change the details of the calculation, but should not change the general trend.

V. CONCLUSION

To summarize, we have performed time resolved Thomson self-scattering measurements at different locations in the plasma along the laser propagation direction. We have observed a systematic and important variation of the intensity ratio between the blue and the red ion spectral components, depending on whether the location of the probed region is in front of or behind the focal plane. Comparing the experimental data with a simple theoretical calculation of Thomson scattering, we have found that this behavior can be qualitatively understood in terms of a deformation of the electron distribution function induced by the classical heat-flux causing a non-Maxwellian distribution. However, a good quantitative agreement is still lacking since our theoretical model predicts significant effects only for ion temperatures that are by a factor of at least two smaller than the values obtained from hydrocode simulations.

ACKNOWLEDGMENTS

The authors gratefully acknowledge S. Glenzer for interest and valuable discussions they had with him. They would also like to thank D. Pesme and W. Rozmus for many fruitful exchanges on this topic.

[1] L. Spitzer and R. Härm, Phys. Rev. **89**, 977 (1953).
[2] P. Mora and J. F. Luciani, Laser Part. Beams **12**, 387 (1994) and references therein; J. F. Luciani, P. Mora, and J. Virmont, Phys. Rev. Lett. **51**, 1664 (1983).
[3] E. E. Salpeter, Phys. Rev. **120**, 1528 (1960).
[4] J. A. Fejer, Can. J. Phys. **38**, 1114 (1960).
[5] H. J. Kunze, in *Plasma Diagnostics*, edited by W. Lochte-Holtgreven (North-Holland, Amsterdam, 1968), p. 550.
[6] J. Sheffield, *Plasma Scattering of Electromagnetic Radiation* (Academic, New York, 1975).
[7] J. E. Bernard *et al.*, Phys. Fluids **30**, 3616 (1987).
[8] M. D. Tracy *et al.*, Phys. Fluids B **4**, 1576 (1992).
[9] J. R. Marquès *et al.*, Phys. Fluids B **5**, 597 (1993).
[10] B. La Fontaine *et al.*, Phys. Plasmas **1**, 2329 (1994).
[11] C. Labaune *et al.*, Phys. Rev. Lett. **75**, 248 (1995).
[12] S. H. Glenzer *et al.*, Phys. Rev. Lett. **77**, 1496 (1996).

[13] V. Malka *et al.*, Phys. Rev. Lett. **79**, 2979 (1997).
[14] S. H. Glenzer *et al.*, Phys. Rev. Lett. **82**, 97 (1999).
[15] E. De Wispelaere *et al.*, Phys. Rev. E **59**, 2322 (1999).
[16] S. D. Baton *et al.*, Phys. Rev. E **57**, R4895 (1998); V. Malka *et al.*, *Rapport d'activité LULI 1996* (Ecole Polytechnique, Palaiseau, France, 1997), NTIS: PB97-170963, p. 13.
[17] B. B. Afeyan *et al.*, Phys. Rev. Lett. **80**, 2322 (1998).
[18] J. F. Myatt *et al.*, Phys. Rev. E **57**, 3383 (1998).
[19] S. Chapman and T. G. Cowling, *The Mathematical Theory of Non-Uniform Gases* (Cambridge University Press, Cambridge, England, 1970).
[20] L. Bhatnagar, E. P. Gross, and M. Krook, Phys. Rev. **94**, 511 (1954); E. P. Gross and M. Krook, *ibid.* **102**, 593 (1956).
[21] N. A. Krall and A. W. Trivelpiece, *Principles of Plasma Physics* (San Francisco Press, Inc., San Francisco, 1986), p. 477.
[22] R. Ramis, R. Schmalz, and J. Meyer-Ter-Vehn, Comput. Phys. Commun. **49**, 475 (1988).
[23] C. T. Dum, Phys. Fluids **21**, 945 (1978); A. B. Langdon, Phys. Rev. Lett. **44**, 575 (1980); P. Alaterre, J. P. Matte, M. Lamoureux, Phys. Rev. A **34**, 1578 (1986); J. P. Matte *et al.*, Plasma Phys. Controlled Fusion **30**, 1665 (1988).